Atmospheric
Chemistry
and Physics

Supplement of

Two distinct ship emission profiles for organic-sulfate source apportionment of PM in sulfur emission control areas

Kirsten N. Fossum et al.

Correspondence to: Jurgita Ovadnevaite (jurgita.ovadnevaite@universityofgalway.ie)

S1 Supplementary Discussion

S1.1 Unconstrained PMF

The PMF solution is a set of factor profiles represented by the corresponding mass spectra and time series. PMF is unconstrained when no *a priori* information about existing source profiles is used to obtain a mathematically reasonable solution. However, a mathematically reasonable solution is not necessarily physically reasonable (Canonaco et al., 2013) and unconstrained PMF can sometimes experience difficulties in separating aerosol sources with temporal covariations, resulting in unrealistic or highly mixed factors (Canonaco et al., 2013). Usually, interpretation of the factors (i.e., source types) is carried out with reference to the mass spectral profiles (e.g., biomass burning) or diurnal cycles (e.g., traffic emissions) of the known sources (Ulbrich et al., 2009) to conclude if the solution is physically reasonable.

When sea-salt aerosol is significant, a known fragmentation pattern of m/z 38, 58, 60, and 83 in order of decreasing relative intensity (sea salt constituents, e.g. $^{23}Na^{35}Cl^+$) appears in the unconstrained PMF. However, no sea-salt fragmentation pattern appeared in the unconstrained factors (2-10) from the Dublin Port dataset.

Using the high time resolution organic species, unconstrained PMF was attempted on the dataset and 2-10 factors were tested. The solution of two – three unconstrained factors resulted in combined factors, including a hydrocarbon-like OA (HOA) factor, an aged or oxidised OA (OOA) factor, and another potentially split factor type of heavier ions (Figure S2a). The unconstrained PMF solutions resulted in mixed factors or splitting between factors such as HOA-like at after three factors (see Figure S2b for e.g. six factors). In this way, unconstrained PMF revealed what was expected, that there was an oil or petrol burning source (HOA) with a possible splitting of heavier ions, and a secondary OA (OOA) consistent with regional pollution found in Dublin (Ovadnevaite et al., 2021; Lin et al., 2019; Lin et al., 2018). However, the disparate yet overlapping primary sources of ship emissions, shipping related traffic, and shipping activities had not been successfully extracted, nor of the secondary formation of Dublin city OOA and port related OOA if any. The former lack of success with unconstrained PMF points to ship fuels having a chemical signature similar to HOA that are intrinsically linked, so the PMF cannot mathematically separate different fuel types (e.g. different types of ship fuels, diesel, or oil burning) using only UMR m/z less than 120. However, the primary sources at the port were resolved by use of constrained profiles.

S1.2 SO_4^{2-} ions

There was a remaining issue with separating the SO_4^{2-} from ship plumes and from regional secondary formation. Within the PMF, the S-Ship factor is being apportioned this SO_4^{2-} from regional secondary formation. The issue arises from the lack of substantial variation within the SO_4^{2-} fragmentation profile (UMR). This lack of variation in the fragmentation profile exists even for degrees of neutralisation of the SO_4^{2-} aerosol measured in controlled lab conditions (Chen et al., 2019). Over the PortAIR intensive campaign, SO_4^{2-} during the exemplary S-Ship plumes (Table S1) was acidic. These SO_4^{2-} profiles can be compared against those during six prominent regional secondary pollution episodes when most SO_4^{2-} was in the form of neutralised ammonium sulfate (Figure S14). Overall, the variation at each m/z can be explained by the sample standard deviation of the mean, except at m/z 80, 81, and 98 (SO_3, HSO_3, and H_2SO_4, respectively). Of these three ions, only m/z 80 has SNR > 2 (Figure S3). It is likely that the prominent SO_4^{2-} portion of the mass spectrum in the constrained S-Ship profile caused the capture of regional pollution events. This capture of the regional pollution events occurred for all constrained PMF runs from up to 10 factor solutions. Even at higher factor numbers, no regional SO_4^{2-} factor emerged, but rather at 9-10 factors a factor emerged, that represented all SO_4^2 and simply robbed contribution from the S-Ship factor.

The SO_4^{2-} fragment ions included in the PMF were m/z 48 for SO^+, m/z 64 for SO_2^+, m/z 80 for SO_3^+, m/z 81 for HSO_3^+, and m/z 98 for $H_2SO_4^+$ (Sun et al., 2012), which account for about 54% of the measured SO_4^{2-} (Figure S4a). The remaining SO_4^{2-} was added back in later to the factors containing SO_4^{2-}, using the ion ratio to m/z 80. The S-Ship factor and OOA factor contained all significant fractions of the SO_4^{2-} ions (Figure 3a), so these factors were affected by the re-addition of the non-measured SO_4^{2-} fragments (see Methods). The S-Ship factor was scaled by a ratio of 1.42 and OOA was scaled by 1.18.

Supplementary Tables

Table S1. Characteristics of the exemplary plumes selected for determining the mean emission profile for both S-Ship and O-Ship types.

Type	Start	End	Duration	SO_2 Mean ($\mu g/m^3$)	OA mean ($\mu g/m^3$)	SO_4^{2-} mean ($\mu g/m^3$)	PM_1 mean ($\mu g/m^3$)	Wind speed (m/s)	Wind direction (°)
S-Ship	19/12/2022 23:20	19/12/2022 23:32	12 min	8.2 ±0.3	17 ±3	21 ±3	44 ±6	3.5 ±0.5	158 ±4
	29/12/2022 20:53	29/12/2022 21:04	11 min	16.1 ±7.6	40 ±20	45 ±11	91 ±34	3.8 ±0.8	173 ±8
	13/01/2023 18:18	13/01/2023 18:35	17 min	No data	22 ±4	29 ±3	53 ±3	4.0 ±0.6	174 ±1
	21/01/2023 05:51	21/01/2023 05:57	6 min	87.9 ±0.3	47 ±8	62 ±4	113 ±12	4.6 ±0.5	169 ±14
	24/01/2023 17:33	24/01/2023 17:44	11 min	5.5 ±1.6	7 ±2	11 ±5	23 ±8	0.2 ±0.3	192±0.1
O-Ship	23/12/2022 20:27	23/12/2022 20:33	6 min	7.0 ±2.1	95 ±14	2 ±1	105 ±16	2.6 ±0.4	252 ±22
	01/01/2023 01:29	01/01/2023 01:35	6 min	6.2 ±0.7	89 ±32	2.1 ±0.9	95 ±32	3.1 ±0.5	235 ±8
	06/01/2023 05:36	06/01/2023 05:43	7 min	9.8 ±1.8	87.4 ±0.8	3.7 ±0.3	98 ±1	3.7 ±0.8	230 ±18
	08/01/2023 11:54	08/01/2023 12:06	12 min	8.0 ±1.0	138 ±23	2.5 ±0.4	145 ±24	4.4 ±0.4	222 ±6
	08/01/2023 14:37	08/01/2023 14:43	6 min	8.2 ±0.3	101 ±6	2 ±1	112 ±5	4.0 ±0.9	221 ±2

Over the full campaign (Dec 2021 – Feb 2023), SO_2 had a median value of 0.921 $\mu g/m^3$, with a 25th – 75th percentile range of 0.457 – 1.564, and a 10th – 90th percentile range of 0.116 – 2.569 $\mu g/m^3$. The standard deviation is $\sigma = 1.5116$, and $3\sigma = 4.5348$. Meaning that the values in Table S1 for all ship plume cases have peak SO_2 concentrations far outside the normal 3σ, and can be considered elevated concentrations. Over the intensive campaign Ni had a median value of 0.0017 $\mu g\ m^{-3}$, and V had a median value of 0.0012 $\mu g\ m^{-3}$ at hourly resolution.

Table S2. Mean characteristics of ship plumes associated with S-Ship (58 plumes) and O-Ship (190 plumes) source apportioned factors. Median values in blue.

	Plume number	Plume number $PM_1 \geq 50$	PM_1 ($\mu g/m^3$)	N (/cm^3)	NO_x ($\mu g/m^3$)	SO_2 ($\mu g/m^3$)	eBC ($\mu g/m^3$)	V/Ni	V ($\mu g/m^3$)	Ni ($\mu g/m^3$)
S-Ship	58	10	29 ± 22 21	$(1.52 \pm 1.55) \times 10^4$ 21.09×10^4	117.6 ± 118.0 83	3.5 ± 3.4 2.4	1.8 ± 1.4 1.3	3.41 ± 0.28 3.47	0.21 ± 0.15 0.17	0.060 ± 0.042 0.050
O-Ship	190	33	32 ± 26 25	$(3.75 \pm 2.28) \times 10^4$ 3.20×10^4	132.3 ± 108.7 97	3.9 ± 3.2 3.0	3.0 ± 1.8 2.7	0.74 ± 0.35 0.71	$(7 \pm 6) \times 10^{-3}$ 5×10^{-3}	$(8 \pm 7) \times 10^{-3}$ 7×10^{-3}

Supplementary Figures

Figure S1. (a) Overview map of Dublin Port (satellite image credit: Imagery ©2024 Airbus, Landsat/Copernicus, Maxar Technologies, Map data ©2024 Google) (top) and (b) an image of the main container with the Xact container *in-situ* (bottom).
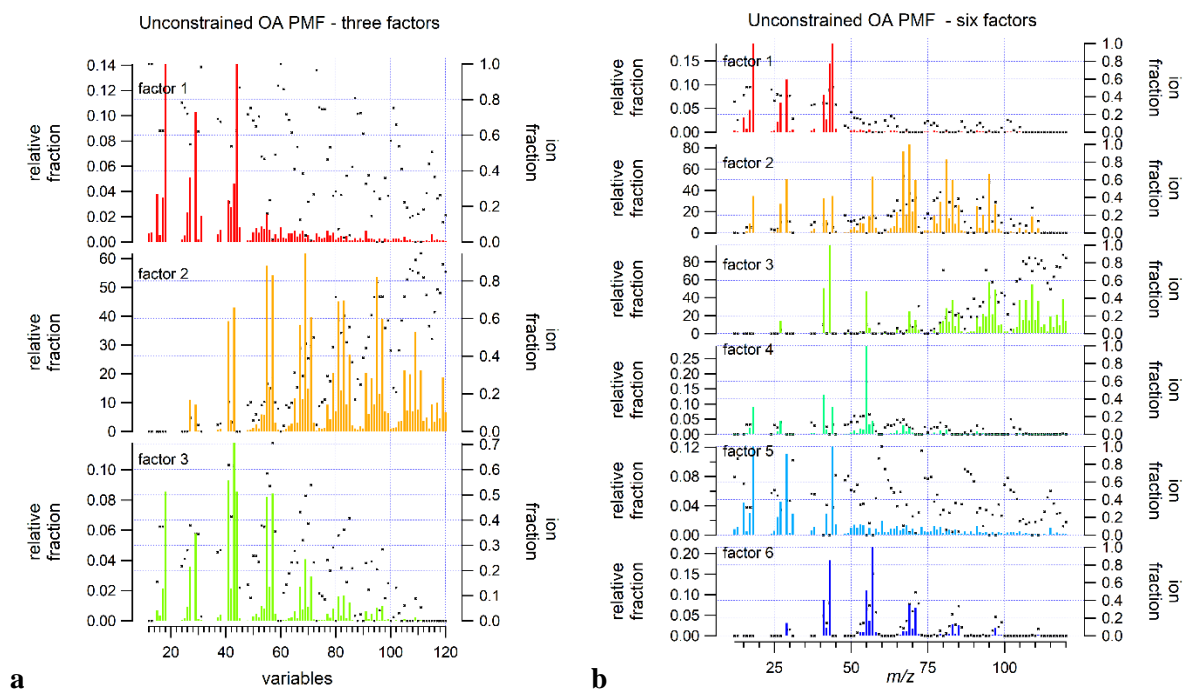
Figure S2. The factor profiles of the unconstrained OA PMF solution of six factors from PortAIR. Left axis is the relative ion fraction of the mass spectrum. Right axis is the relative ion fraction contained in that profile compared with the total (markers).
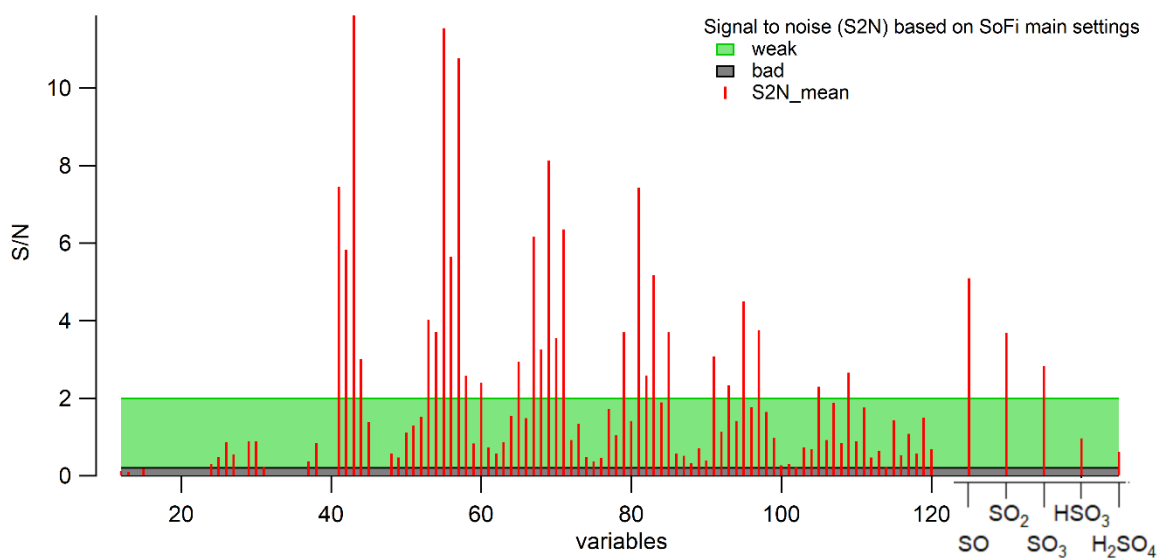
Figure S3. SNR plot of fragment OA and SO_4^{2-} ions. Weak ions are considered $2 > SNR > 0.2$ (green band), while bad ions $SNR < 0.2$ (grey band).
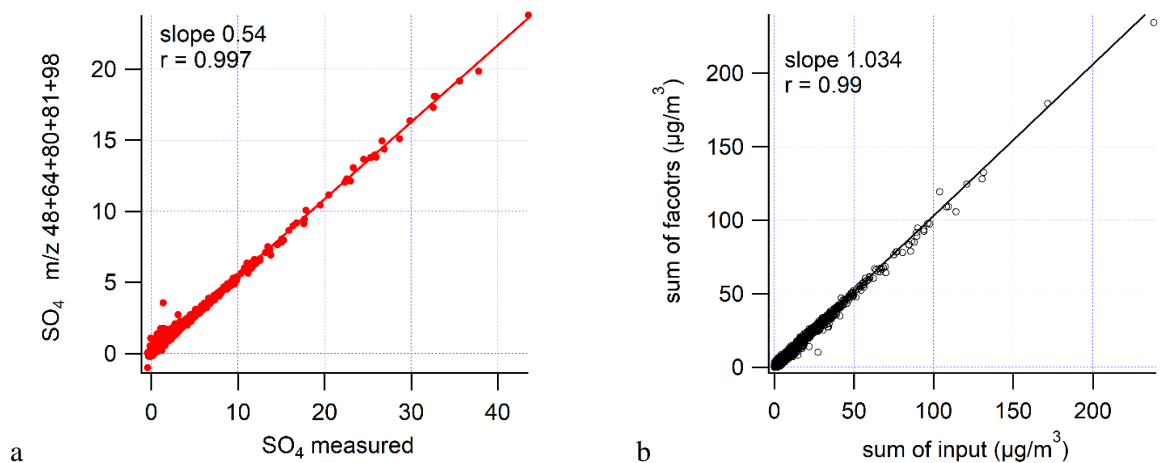
Figure S4. Scatter plot of the mass concentration of the (a) input SO$_4^{2-}$ ions *vs* the SO$_4^{2-}$ measured, and (b) organic-sulfate factors (sum of factors) *vs* the input for PMF of the OA + SO$_4^{2-}$ mass concentration (line shows linear regression fit).
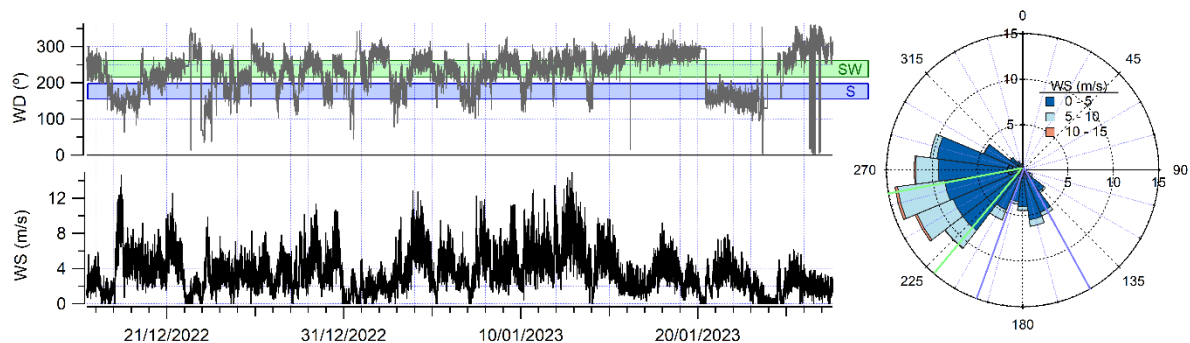
Figure S5. (Left) Time series of wind direction (WD) and wind speed (WS) over the intensive campaign. (Right) Polar plot of the probability distribution (radial axis) of wind direction (degrees in angle axis, with WS indicated by color). The WD across Berth SW, and Berth S, are indicated by the green and blue highlighted regions, respectively.
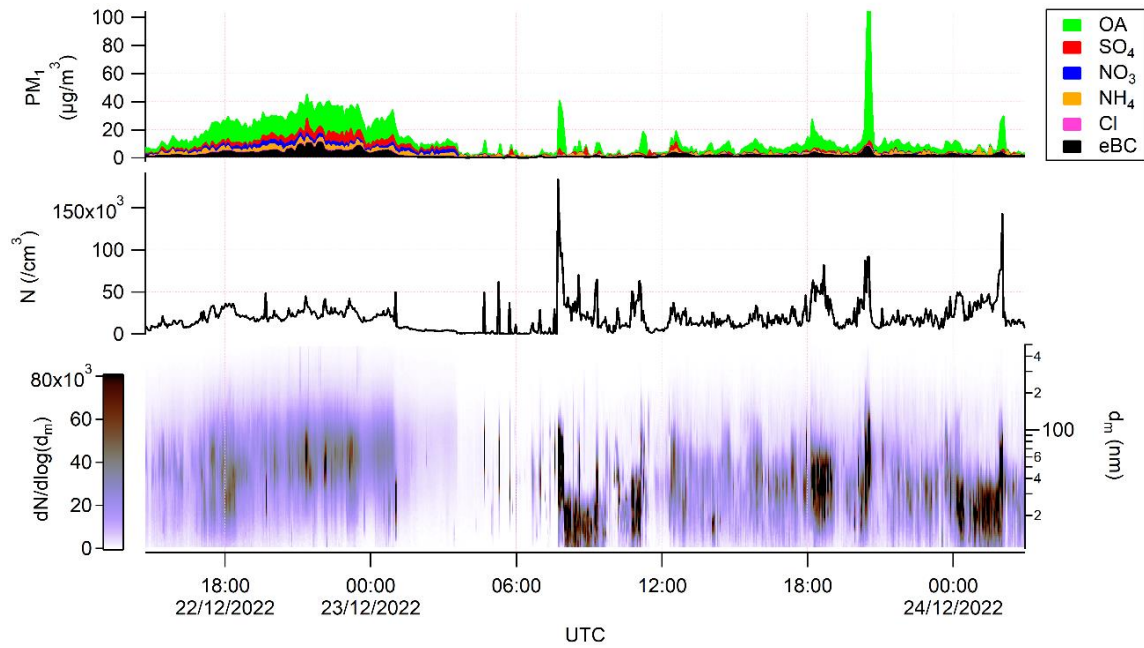
Figure S6. Excerpt time series of the high-resolution ambient measurements from PortAIR during the intensive month (December 22 – 24, 2022). From top to bottom panels, reconstructed PM$_1$ (NR-PM$_1$ species + eBC) displayed as species stacked on top of each other, the number concentration (N) of particles from 10-500 nm in dry electrical mobility diameter (d$_m$) from the SMPS, and the curtain plot of the SMPS data, right axis shows d$_m$ with the color indicating the number concentration (dN/dlog(d$_m$)) of particles at that size.
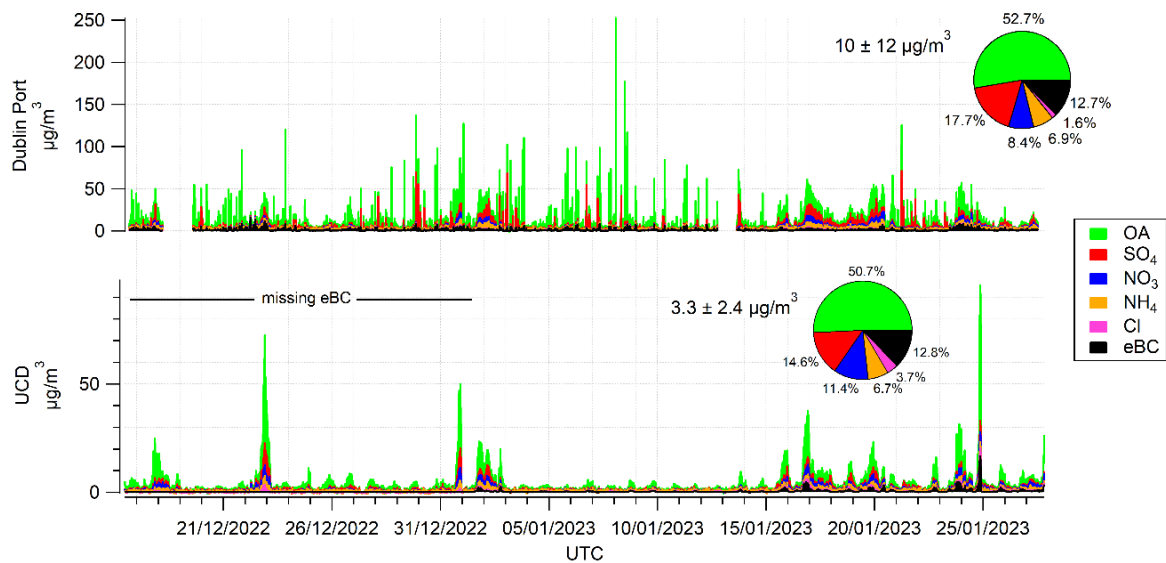
Figure S7. PM$_1$ time series of the Dublin Port Q-ACSM and AE33 data (top panel) and of the established Dublin urban background site at UCD (bottom panel). Note that the vertical axis scales are different to make the UCD data viewable.
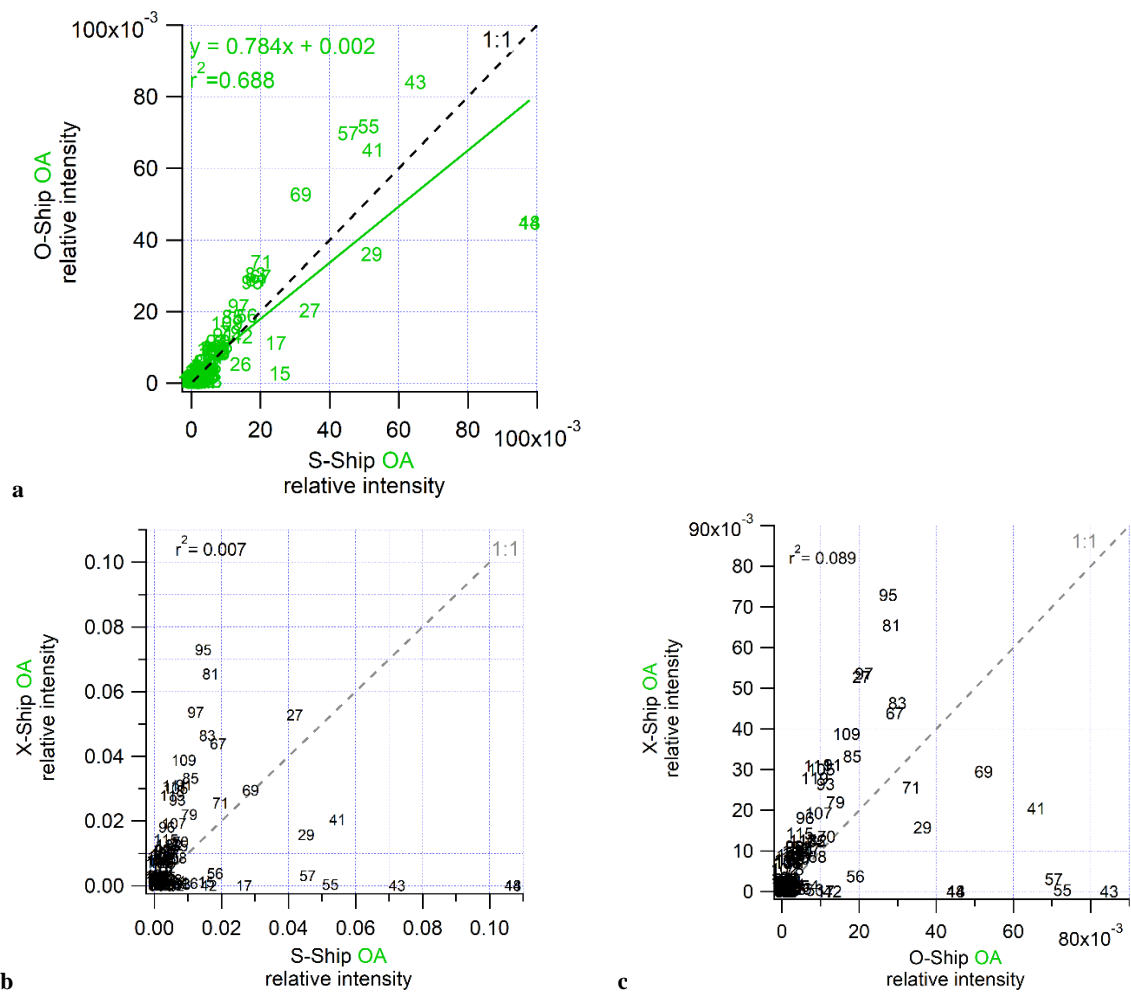
Figure S8. Scatter plots of relative intensities of OA ions of (a) O-Ship versus S-Ship mass spectrum, (b) X-Ship versus S-Ship, and (c) X-Ship versus O-Ship mass spectra. The 1:1 dashed line (grey), while the ions are shown as numbered markers representing the m/z (UMR) of each ion.
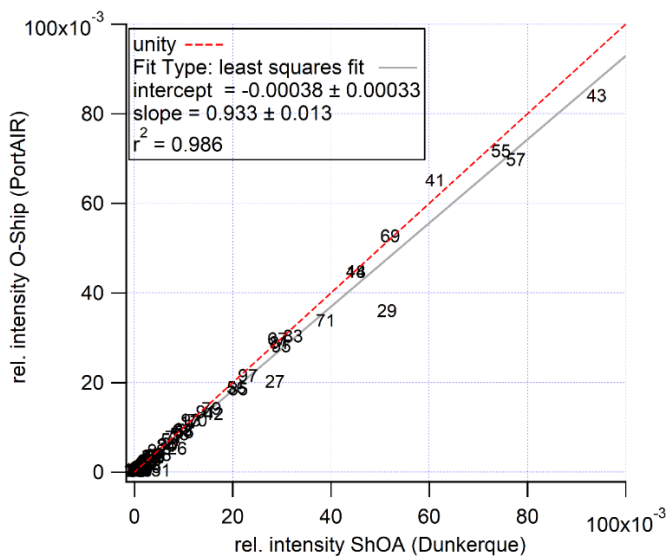
Figure S9. Scatter plot of the relative intensities of the OA ions of the O-Ship factor compared to the Dunkerque campaign Ship-like organic aerosol (ShOA) (Zhang, 2016). The marker numbers are the *m/z* of the ions.
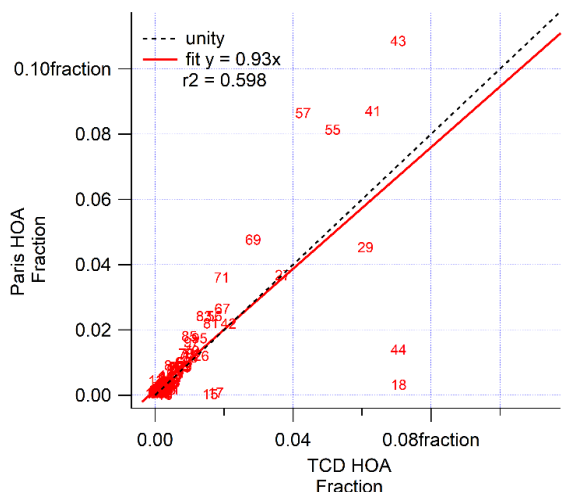
Figure S10. Scatter plot of the relative ion intensities of the classic Paris HOA Fraction (Crippa et al., 2013) compared to the HOA derived from the curb side in Dublin, Ireland (TCD HOA). This uses a different PM$_1$ Q-ACSM from the intensive campaign. The marker numbers are the *m/z* of the ions.
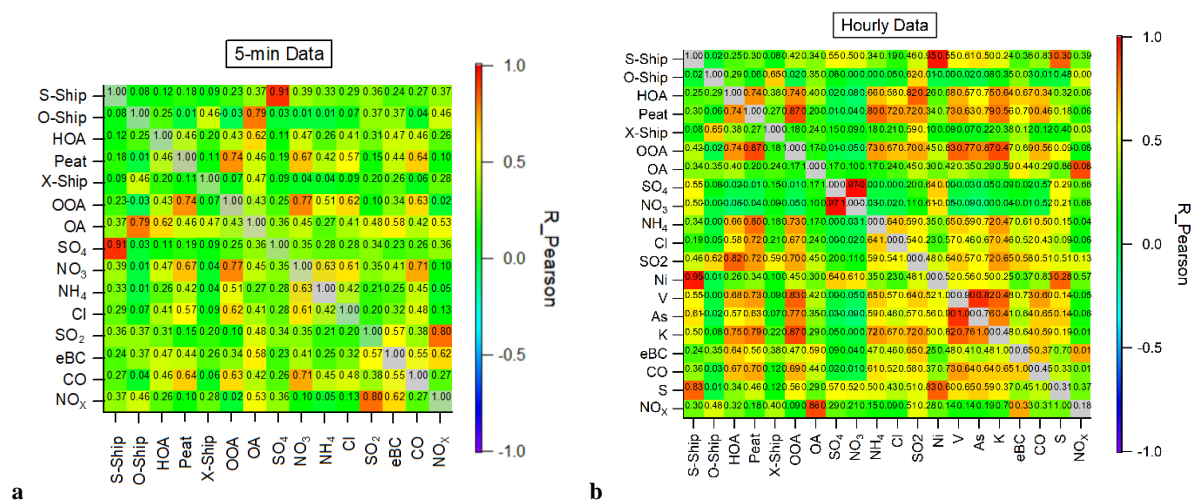
Figure S11. Correlation matrix of the time series of PMF factors and other (external) species at (a) native time resolution of the Q-ACSM, and (b) at hourly time resolution.
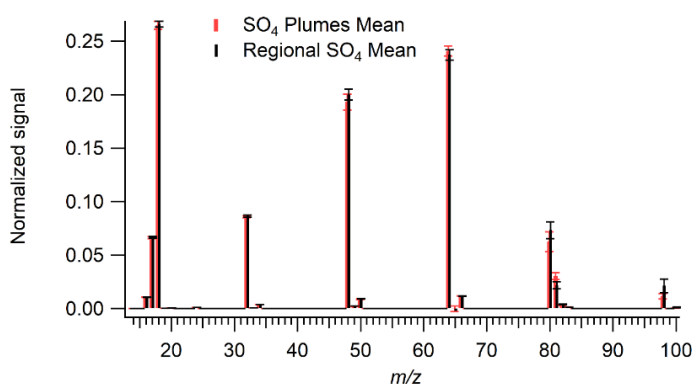
Figure S12. Mean mass spectrum of the SO$_4^{2-}$ ion fragments for the regional ammonium sulfate (black) and for acidic sulfate plumes from the exemplary S-Ship cases (red). Standard deviation of the sample shown in error bars.
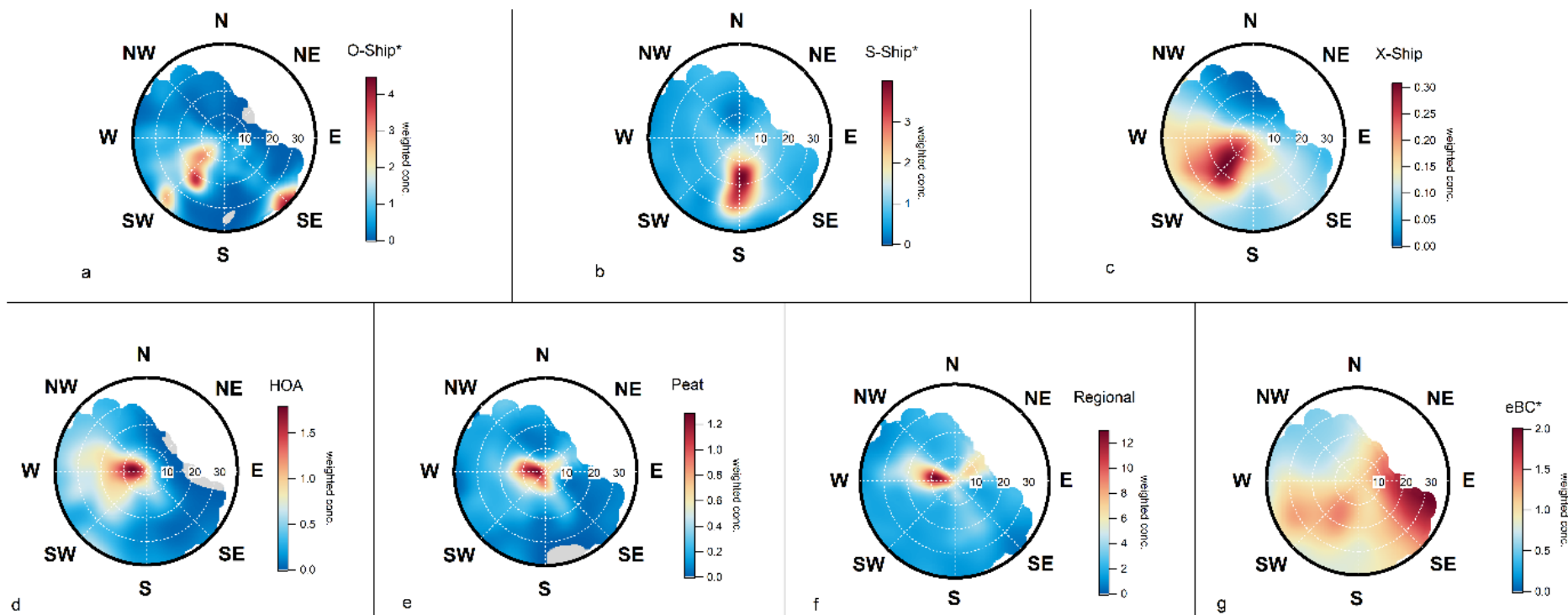
Figure S13. Pollution roses plotted using the statistical mean in the Openair package in R of the apportioned sources including (a) O-Ship*, (b) S-Ship*, (c) X-Ship, (d) HOA, (e) peat, (f) regional, and (g) eBC*. The color denotes the weighted concentration of the species based on wind direction and speed.
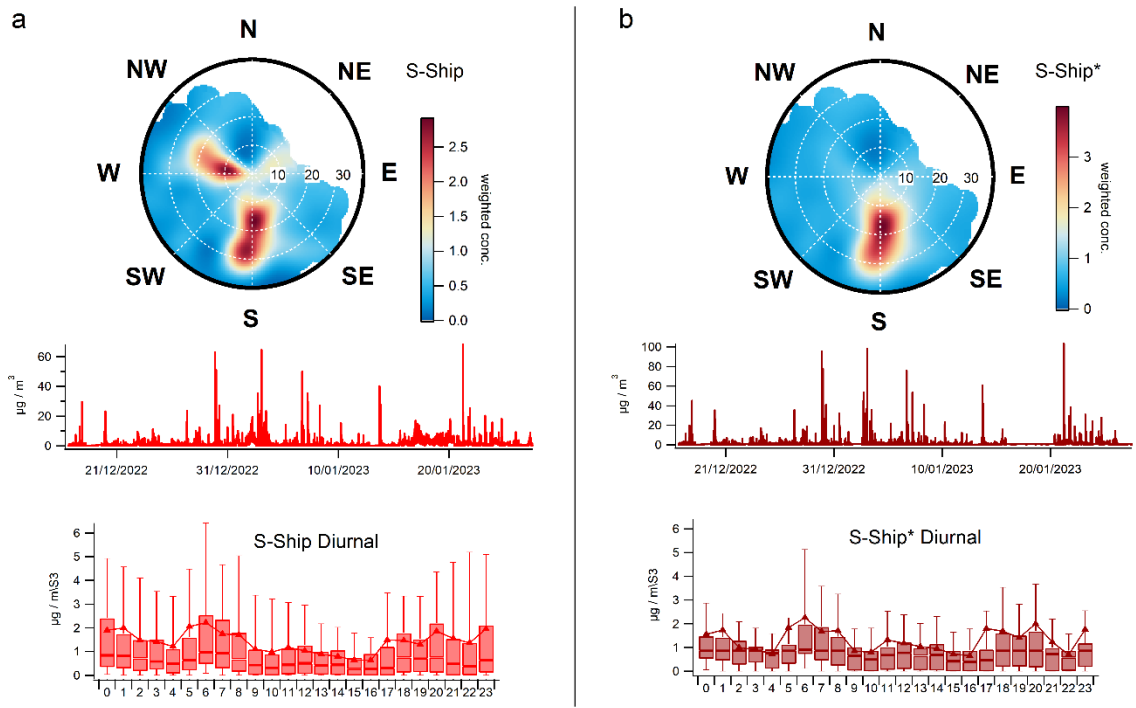
Figure S14. Graphs show differences in (a) the S-Ship PMF factor (b) the S-Ship* source contribution estimate obtained by subtracting regional sulfate from S-Ship. (Top) Pollution roses plotted using the statistical mean in the Openair package in R where the color denotes the weighted concentration of the species based on wind direction and speed. (Middle) Time series of the data. (Bottom) Diurnal trends of the data (mass concentration vs hour of the day) with triangle markers and error bars showing mean and standard deviation, and box plots showing medians and percentiles.
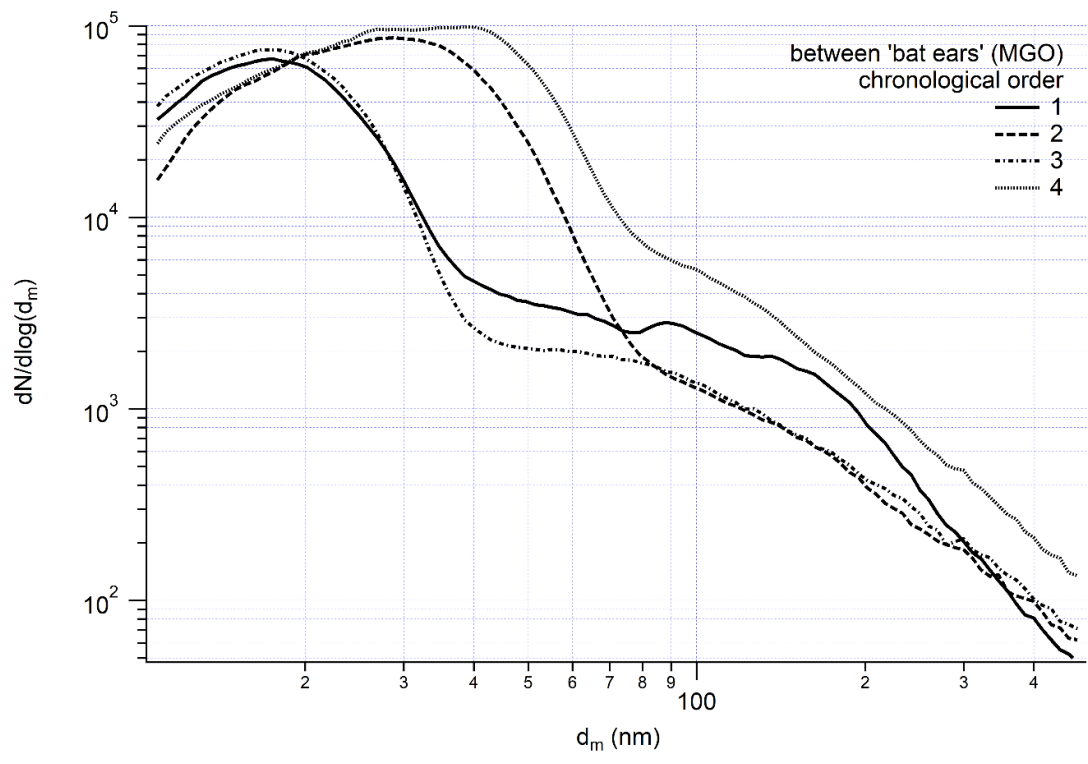
Figure S15. Averaged number-size distributions of particles observed from MGO emissions during the four hoteling periods (between the 'bat ears') in Figure 7a. Data is shown as the lognormal particle concentration (dN/dlog(d_m)) *vs* dry electrical mobility diameter (d_m) in nm.

Supplementary References

Canonaco, F., Crippa, M., Slowik, J. G., Baltensperger, U., and Prévôt, A. S. H.: SoFi, an IGOR-based interface for the efficient use of the generalized multilinear engine (ME-2) for the source apportionment: ME-2 application to aerosol mass spectrometer data, Atmos. Meas. Tech., 6, 3649-3661, 10.5194/amt-6-3649-2013, 2013.

Chen, Y., Xu, L., Humphry, T., Hettiyadura, A. P. S., Ovadnevaite, J., Huang, S., Poulain, L., Schroder, J. C., Campuzano-Jost, P., Jimenez, J. L., Herrmann, H., O'Dowd, C., Stone, E. A., and Ng, N. L.: Response of the Aerodyne Aerosol Mass Spectrometer to Inorganic Sulfates and Organosulfur Compounds: Applications in Field and Laboratory Measurements, Environmental Science & Technology, 53, 5176-5186, 10.1021/acs.est.9b00884, 2019.

Crippa, M., El Haddad, I., Slowik, J. G., DeCarlo, P. F., Mohr, C., Heringa, M. F., Chirico, R., Marchand, N., Sciare, J., Baltensperger, U., and Prévôt, A. S. H.: Identification of marine and continental aerosol sources in Paris using high resolution aerosol mass spectrometry, Journal of Geophysical Research: Atmospheres, 118, 1950-1963, doi:10.1002/jgrd.50151, 2013.

Lin, C., Huang, R.-J., Ceburnis, D., Buckley, P., Preissler, J., Wenger, J., Rinaldi, M., Facchini, M. C., O'Dowd, C., and Ovadnevaite, J.: Extreme air pollution from residential solid fuel burning, Nature Sustainability, 1, 512-517, 10.1038/s41893-018-0125-x, 2018.

Lin, C., Ceburnis, D., Huang, R. J., Xu, W., Spohn, T., Martin, D., Buckley, P., Wenger, J., Hellebust, S., Rinaldi, M., Facchini, M. C., O'Dowd, C., and Ovadnevaite, J.: Wintertime aerosol dominated by solid-fuel-burning emissions across Ireland: insight into the spatial and chemical variation in submicron aerosol, Atmos. Chem. Phys., 19, 14091-14106, 10.5194/acp-19-14091-2019, 2019.

Ovadnevaite, J., Lin, C., Rinaldi, M., Ceburnis, D., Buckley, P., Coleman, L., Facchini, M. C., Wenger, J., and O'Dowd, C.: Air Pollution Sources in Ireland; 2016-CCRP-MS.31, National University of Ireland Galway, Istituto di Scienze dell'Atmosfera e del Clima and University College Cork www.epa.ie, 60, 2021.

Sun, Y. L., Zhang, Q., Schwab, J. J., Yang, T., Ng, N. L., and Demerjian, K. L.: Factor analysis of combined organic and inorganic aerosol mass spectra from high resolution aerosol mass spectrometer measurements, Atmos. Chem. Phys., 12, 8537-8551, 10.5194/acp-12-8537-2012, 2012.

Ulbrich, I. M., Canagaratna, M. R., Zhang, Q., Worsnop, D. R., and Jimenez, J. L.: Interpretation of organic components from Positive Matrix Factorization of aerosol mass spectrometric data, Atmos. Chem. Phys., 9, 2891-2918, 10.5194/acp-9-2891-2009, 2009.

Zhang, S.: Dynamic analysis, in near field and with a finer temporal resolution, of a sub-micron aerosol in urban situation under industrial influence - Analyse dynamique, en champ proche et à résolution temporelle fine, de l'aérosol submicronique en situation urbaine sous influence industrielle, Université du Littoral Côte d'Opale, 2016.